Searches for Double Beta Decay of ^{134}Xe with EXO-200

(EXO-200 Collaboration)

J.B. Albert,[1] G. Anton,[2] I. Badhrees,[3,*] P.S. Barbeau,[4] R. Bayerlein,[2] D. Beck,[5] V. Belov,[6] M. Breidenbach,[7] T. Brunner,[8,9] G.F. Cao,[10] W.R. Cen,[10] C. Chambers,[11] B. Cleveland,[12,13] M. Coon,[5] A. Craycraft,[11] W. Cree,[3] T. Daniels,[7] M. Danilov,[6,†] S.J. Daugherty,[1] J. Daughhetee,[14] J. Davis,[7] S. Delaquis,[7] A. Der Mesrobian-Kabakian,[12] R. DeVoe,[15] T. Didberidze,[16] J. Dilling,[9] A. Dolgolenko,[6] M.J. Dolinski,[17] W. Fairbank Jr.,[11] J. Farine,[12] S. Feyzbakhsh,[18] P. Fierlinger,[19] D. Fudenberg,[15] R. Gornea,[3,9] K. Graham,[3] G. Gratta,[15] C. Hall,[20] J. Hoessl,[2] P. Hufschmidt,[2] M. Hughes,[16] A. Jamil,[2,15] M.J. Jewell,[15] A. Johnson,[7] S. Johnston,[18,‡] A. Karelin,[6] L.J. Kaufman,[1] T. Koffas,[3] S. Kravitz,[15] R. Krücken,[9] A. Kuchenkov,[6] K.S. Kumar,[21] Y. Lan,[9] D.S. Leonard,[22] S. Li,[5] C. Licciardi,[3] Y.H. Lin,[17] R. MacLellan,[14] M.G. Marino,[19] T. Michel,[2] B. Mong,[7] D. Moore,[23] K. Murray,[8] R. Nelson,[24] O. Njoya,[21] A. Odian,[7] I. Ostrovskiy,[16] A. Piepke,[16] A. Pocar,[18] F. Retière,[9] P.C. Rowson,[7] J.J. Russell,[7] A. Schubert,[15] D. Sinclair,[3,9] E. Smith,[17] V. Stekhanov,[6] M. Tarka,[21] T. Tolba,[10] R. Tsang,[16,§] P. Vogel,[25] J.-L. Vuilleumier,[26] M. Wagenpfeil,[2] A. Waite,[7] J. Walton,[5] T. Walton,[11] M. Weber,[15] L.J. Wen,[10] U. Wichoski,[12] L. Yang,[5] Y.-R. Yen,[17] O.Ya. Zeldovich,[6] J. Zettlemoyer,[1] and T. Ziegler[2]

[1] *Physics Department and CEEM, Indiana University, Bloomington, Indiana 47405, USA*
[2] *Erlangen Centre for Astroparticle Physics (ECAP), Friedrich-Alexander-University Erlangen-Nürnberg, Erlangen 91058, Germany*
[3] *Physics Department, Carleton University, Ottawa, Ontario K1S 5B6, Canada*
[4] *Department of Physics, Duke University, and Triangle Universities Nuclear Laboratory (TUNL), Durham, North Carolina 27708, USA*
[5] *Physics Department, University of Illinois, Urbana-Champaign, Illinois 61801, USA*
[6] *Institute for Theoretical and Experimental Physics, Moscow, Russia*
[7] *SLAC National Accelerator Laboratory, Menlo Park, California 94025, USA*
[8] *Physics Department, McGill University, Montréal, Québec H3A 2T8, Canada*
[9] *TRIUMF, Vancouver, British Columbia V6T 2A3, Canada*
[10] *Institute of High Energy Physics, Beijing, China*
[11] *Physics Department, Colorado State University, Fort Collins, Colorado 80523, USA*
[12] *Department of Physics, Laurentian University, Sudbury, Ontario P3E 2C6, Canada*
[13] *SNOLAB, Sudbury, Ontario P3Y 1N2, Canada*
[14] *Physics Department, University of South Dakota, Vermillion, South Dakota 57069, USA*
[15] *Physics Department, Stanford University, Stanford, California 94305, USA*
[16] *Department of Physics and Astronomy, University of Alabama, Tuscaloosa, Alabama 35487, USA*
[17] *Department of Physics, Drexel University, Philadelphia, Pennsylvania 19104, USA*
[18] *Amherst Center for Fundamental Interactions and Physics Department, University of Massachusetts, Amherst, MA 01003, USA*
[19] *Technische Universität München, Physikdepartment and Excellence Cluster Universe, Garching 80805, Germany*
[20] *Physics Department, University of Maryland, College Park, Maryland 20742, USA*
[21] *Department of Physics and Astronomy, Stony Brook University, SUNY, Stony Brook, New York 11794, USA*
[22] *IBS Center for Underground Physics, Daejeon, Korea*
[23] *Department of Physics, Yale University, New Haven, Connecticut 06511, USA*
[24] *Waste Isolation Pilot Plant, Carlsbad, New Mexico 88220, USA*
[25] *Kellogg Lab, Caltech, Pasadena, California 91125, USA*
[26] *LHEP, Albert Einstein Center, University of Bern, Bern, Switzerland*

(Dated: November 7, 2017)

Searches for double beta decay of ^{134}Xe were performed with EXO-200, a single-phase liquid xenon detector designed to search for neutrinoless double beta decay of ^{136}Xe. Using an exposure of 29.6 kg·yr, the lower limits of $T^{2\nu\beta\beta}_{1/2} > 8.7 \cdot 10^{20}$ yr and $T^{0\nu\beta\beta}_{1/2} > 1.1 \cdot 10^{23}$ yr at 90% confidence level were derived, with corresponding half-life sensitivities of $1.2 \cdot 10^{21}$ yr and $1.9 \cdot 10^{23}$ yr. These limits exceed those in the literature for ^{134}Xe, improving by factors of nearly 10^5 and 2 for the two antineutrino and neutrinoless modes, respectively.

* Permanent with King Abdulaziz City for Science and Technology, Riyadh, Saudi Arabia
† Now at P.N.Lebedev Physical Institute of the Russian Academy of Sciences, Moscow, Russia
‡ Now at Argonne National Laboratory, Argonne, Illinois USA
§ Now at Pacific Northwest National Laboratory, Richland, Washington, USA

I. INTRODUCTION

This paper presents the search for two modes of double beta ($\beta\beta$) decay of ^{134}Xe. $\beta\beta$ decay is a second-order weak transition between two nuclei with the same mass number and nuclear charges that differ by two units. This process can only be observed if the single beta (β) decay is strongly suppressed or forbidden by energy conservation. The mode with emission of two antineutrinos and two electrons ($2\nu\beta\beta$) is an allowed decay by the Standard Model (SM) and has been directly observed in nine nuclei [1]. Among them, ^{136}Xe presents the longest half-life of $2.165 \pm 0.016\,(\text{stat.}) \pm 0.059\,(\text{syst.}) \cdot 10^{21}$ yr [2]. The hypothetical neutrinoless mode with emission of two electrons and nothing else ($0\nu\beta\beta$) does not conserve lepton number and, if observed, would imply that neutrinos are massive Majorana particles [3]. The most stringent lower limits derived for the half-life of $0\nu\beta\beta$ in ^{136}Xe are $1.1 \cdot 10^{26}$ yr [4] and $1.1 \cdot 10^{25}$ yr [5] at 90% confidence level (CL).

The $\beta\beta$ decay of ^{134}Xe into ^{134}Ba:

$$^{134}\text{Xe} \rightarrow ^{134}\text{Ba}^{++} + 2\,e^- \,(+2\,\bar{\nu}_e)\ ,$$

has a Q-value of 825.8 ± 0.9 keV [6] and neither of the two $\beta\beta$ modes have been observed to date. Because $\beta\beta$ decay rates scale strongly with the Q-value: $\sim Q^{11}$ in $2\nu\beta\beta$ and $\sim Q^5$ in $0\nu\beta\beta$ [7, 8], experimental searches have favored ^{136}Xe (Q-value of 2457.83 ± 0.37 keV [9]). Moreover, in xenon detectors containing both isotopes, ^{136}Xe $2\nu\beta\beta$ produces a background that makes the $\beta\beta$ searches in ^{134}Xe even more challenging. The current experimental limit for the half-life of $2\nu\beta\beta$ in ^{134}Xe is $\text{T}^{2\nu\beta\beta}_{1/2} > 1.1 \cdot 10^{16}$ yr at 68% CL [10], while theoretical predictions put it in the range of $\sim 10^{24} - 10^{25}$ yr [11]. On the other hand, more recent searches set the most stringent limit for the $0\nu\beta\beta$ half-life at $\text{T}^{0\nu\beta\beta}_{1/2} > 5.8 \cdot 10^{22}$ yr at 90% CL [12].

The searches presented in this paper are rooted in the success of the EXO-200 analyses of $\beta\beta$ decays in ^{136}Xe [2, 5, 13, 14]. Unique to this work, the energy threshold was extended to lower energies as required by the $\beta\beta$ searches in ^{134}Xe. As will be discussed in Sec. III, each decay mode was analyzed independently, using a different energy threshold. The Monte Carlo (MC) simulation and reconstruction processes were improved, as detailed in Sec. II, to further improve the agreement between data and MC. Another change with respect to previous EXO-200 analyses is the use of the full set of data between June 2011, and February 2014, corresponding to a 25% increase in livetime (EXO-200 Phase-I).

II. THE EXO-200 DETECTOR, DATA AND MC SIMULATION

The EXO-200 detector consists of two back-to-back cylindrical single-phase time projection chambers (TPCs), sharing a central cathode, filled with liquid xenon (LXe). The isotopic composition of the LXe is $80.672 \pm 0.014\%$ ^{136}Xe and $19.098 \pm 0.014\%$ ^{134}Xe. The ratio between these two isotopes was measured using dynamic dual-inlet mass spectrometry [15]. In addition, the contamination from other Xe isotopes was measured to be $< 0.25\%$, dominated by a 0.2% contamination of ^{132}Xe. The significant concentration of ^{134}Xe, almost twice its natural abundance of 10.4%, presents a unique opportunity and motivates this work.

The detector is located at the Waste Isolation Pilot Plant (WIPP) in Carlsbad, NM, USA, in a clean room under an overburden of 1624 meters water equivalent. An active muon veto system surrounding the clean room on four sides identifies 96% of the cosmic ray muons passing through the TPCs, and allows rejection of prompt cosmogenic backgrounds [16].

A radiopure copper vessel, nearly 44 cm in length and 40 cm in diameter, contains the EXO-200 TPCs. Each TPC is instrumented near the ends of the vessel with a pair of wire planes, crossed at 60°, in front of an array of silicon large-area avalanche photodiodes (APDs). Ionizing particles passing through the LXe deposit energy that produces both scintillation light ($\sim$ 178 nm wavelength), detected by the APDs almost instantenously, and electron-ion pairs. The electrons are drifted towards the wire grids, inducing signals in the front-most wire plane (V-wires), and then are collected by the second wire plane (U-wires). Copper "field-shaping" rings ensure a sufficient uniformity of the electric field over the bulk of the LXe, and inside them a cylindrical PTFE reflector improves collection efficiency of the scintillation light. A more detailed description of the detector can be found in [17].

All three spatial coordinates (3D) of the energy depositions are reconstructed in EXO-200. Information from the U- and V-wires results in 2D clusters (X and Y coordinates) formed by the charge detection (charge clusters). The time difference between the light signal (scintillation cluster) and associated charge clusters provides their third coordinate (Z). The subcentimeter position resolution [2] provides strong separation between single-site (SS) events, primarily β or $\beta\beta$ decays with characteristic dimension of $\sim 2 - 3$ mm, and multi-site (MS) events, arising mostly from multiple interactions of MeV-energy γ-rays. Furthermore, internally generated β-like events in the fiducial volume (FV) are uniformly distributed in the LXe, in contrast to the spatial distribution of background events arising from γ-rays entering the TPC. This difference is captured in the analysis by the standoff-distance variable, defined as the shortest distance between any event cluster and the closest material that is not LXe, other than the cathode. The event energy is calculated using a linear combination of the measured ionization and scintillation signals that optimizes the energy resolution [18], determined using the 2615 keV γ-line of ^{208}Tl.

Both the spectral fitting analysis, presented in Sec. III,

and detector calibration rely on detailed modeling of the detector response. For these purposes, a GEANT4-based application [19] is part of the EXO-200 MC simulation software, as described in [2]. The collaboration has been gradually implementing changes into this package to better describe the measurements with the detector [13]. For this analysis, the simulation was updated to incorporate three important effects, in order to improve the spectral agreement with data at low energies. First, since electronegative impurities can capture electrons drifting in the LXe, the charge collection is exponentially attenuated with drifting distance before the simulation of the electronics pulse shapes. The average electron lifetime included in the simulation is based on calibration measurements ($\bar{\tau}_e = 4.5$ ms). In addition, a more realistic light response of the APDs is included, which is now based on EXO-200 data to account for the complexity of optical propagation in the detector, such as internal reflections. Finally, the diffusion of the drifting electrons has been incorporated following the EXO-200 measurement of the transverse coefficient in LXe at the nominal drift field of 380 V/cm ($D = 55$ cm^2/s) [20].

The energy calibration relies on data acquired with radioactive γ sources deployed near the detector [2]. The energy scale and resolution are simultaneously determined by fitting the expected energy spectra, as generated by MC, to the corresponding calibration data [13]. These fits were performed with a reduced energy threshold suited for both $\beta\beta$ decay searches of ^{134}Xe. The effective livetime-weighted average of the resolution in this analysis is $\sigma/E = 1.60\%$ and 3.56% for SS events at the Q-value of ^{136}Xe and ^{134}Xe, respectively. To reach this result, a sophisticated de-noising algorithm was developed optimizing the energy resolution in the presence of correlated noise from the APD electronics [21].

The total livetime of the EXO-200 data considered here is 596.7 days. The fiducial volume (FV) is defined by events within 10 mm $< |Z| <$ 182 mm, where $Z = 0$ is the cathode plane, and constrained in a hexagon with 162 mm apothem, centered at $(X, Y) = (0, 0)$. This corresponds to 18.1 kg of ^{134}Xe, *i.e.* $8.14 \cdot 10^{25}$ atoms, which results in an exposure of 29.6 kg·yr (221 mol·yr).

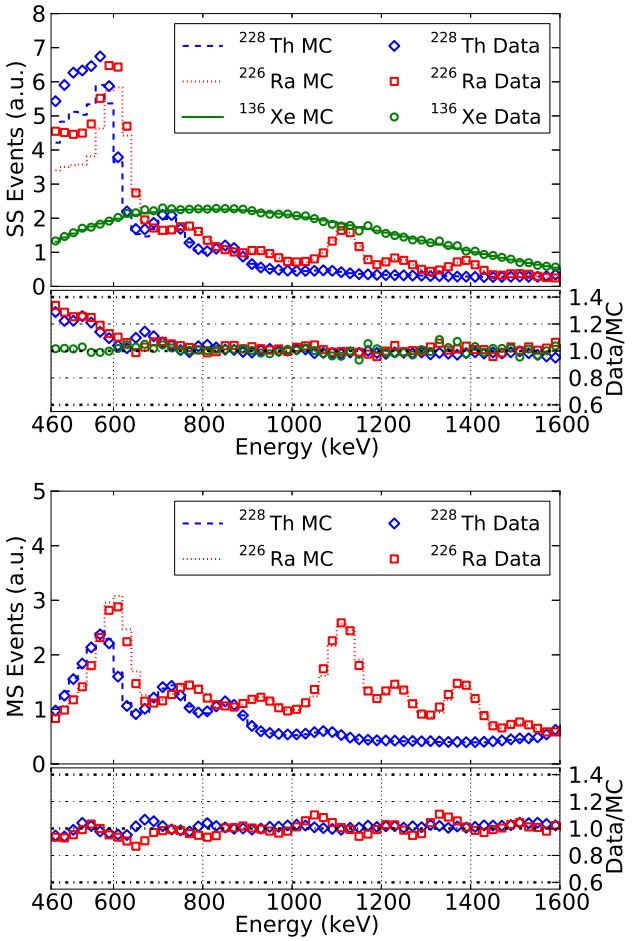

Figure 1. Energy spectral agreement between data and MC simulation in SS (top) and MS (bottom) events. The comparison is presented between 460 keV and 1600 keV for two calibration sources, ^{228}Th and ^{226}Ra, deployed near the cathode of the detector for calibration runs. The background-subtracted ^{136}Xe-$2\nu\beta\beta$ spectrum is compared to MC only in SS events. A worsening of the agreement in SS γ-like spectra is observed for energies $\lesssim 600$ keV. This effect was considered in the searches as discussed in Sec. IV.

III. ANALYSIS PROCEDURE

The low Q-value of the $\beta\beta$ decay of ^{134}Xe requires an energy threshold that is substantially lower than the 980 keV used in other EXO-200 publications. The improvements described in Sec. II produce an agreement between data and MC better than 10% for energies above 600 keV, as shown in Fig. 1. The agreement worsens below this energy and reaches 30% near 460 keV in SS events induced by γ-rays from calibration sources. The effects of these discrepancies are discussed in Sec. IV. The standoff-distance agreement was not observed to degrade at low energies when compared to previous EXO-200 analyses.

Following a similar procedure from previous analyses [2, 5, 13, 14], the search for each $\beta\beta$ decay mode of ^{134}Xe was performed independently using a binned negative log-likelihood (NLL) function to fit simultaneously both SS and MS events with their corresponding probability density functions (PDFs), as generated by MC, in energy and standoff-distance. Five Gaussian constraints, presented in Sec. IV, were included in the NLL function to incorporate the systematic uncertainties independently evaluated for each search, in a similar approach as [2]. The SS fraction of each component, defined by the ratio of the number of SS events to the total number of events (SS/(SS+MS)), parametrizes the proportion of counts assigned to SS and MS PDFs. Unlike previous analyses, these searches used non-uniform bin widths, which optimize the calculation speed without decreasing

the experimental sensitivity. In particular, the standoff-distance binning partitions the LXe in equal volumes. A profile-likelihood scan was then performed to derive the limits at 90% CL using a profile-likelihood ratio (ΔNLL) of 1.35, under the assumption of Wilks's theorem [22, 23], which applies, given the large statistics of the data set in the region of interest.

A fit model comprising the significant components that contribute to events with energies above 700 keV was developed in [2]. At lower energies, two additional components are expected to contribute to backgrounds:

- ^{85}Kr dissolved in the LXe, producing β decays with end point at 687.4 keV;
- ^{137}Cs in the materials near the LXe, with γ-rays of 661.7 keV.

The shape of the simulated $\beta\beta$ decay spectrum of ^{134}Xe is the same as that of ^{136}Xe, with the appropriate Q-value. The simulated energy spectrum of ^{85}Kr includes the two β-decay modes with branching ratios of 99.56% and 0.44% to the ground and excited states of ^{85}Rb, respectively. The latter is followed by the release of a 514 keV γ-ray. A shape correction accounting for the forbidden nature of the first unique β decay was calculated using the method described in [24], and found between -15% and 80% depending on its energy. This correction was applied as an event weighting in the MC simulation.

The possible difference between the energy scale of β- and γ-like events is modeled by a scaling factor, the β-scale. This is a free parameter applied on the β-like PDFs that allows for a possible shift in energy scale between β-like PDFs and the γ calibration sources.

Different energy thresholds are used to optimize the sensitivities for $2\nu\beta\beta$ and $0\nu\beta\beta$ decays. The $2\nu\beta\beta$ decay requires the lowest possible energy threshold, in order to maximize the signal detection efficiency and discrimination power between low-energy backgrounds, while keeping the systematic errors arising from the spectral agreement at reasonable levels. Because all these effects are propagated into the profile-likelihood ratio, the sensitivity (obtained through fits of toy data sets generated by the background model) was evaluated with energy thresholds varying between 400 keV and 500 keV, in steps of 20 keV, and found to be optimal in the region between 460 keV and 480 keV (with negligible differences within this range). The choice of 460 keV can then be motivated by its signal detection efficiency, 5.6% as opposed to 4.5%. On the other hand, the $0\nu\beta\beta$ detection efficiency is nearly maximal, 89%, for all energies below 760 keV. The energy threshold of this search is then selected at 740 keV, sufficiently away from the low-energy background components, even when accounting for the energy resolution. For this reason, the ^{85}Kr and ^{137}Cs PDFs are only included in the fit model of the ^{134}Xe $2\nu\beta\beta$ search.

IV. SYSTEMATIC ERRORS

The five Gaussian constraints added to the NLL, responsible for the propagation of the systematic errors into the searches, correspond to:

- uncertainty in the activity of radon in the LXe as determined in stand-alone studies;
- uncertainty in the relative fractions of neutron-capture-related PDF components generated by dedicated simulations;
- uncertainty in SS fractions as obtained in MC;
- uncertainty in the overall efficiency, also referred to as *normalization*, caused by imperfections in the MC model;
- uncertainty in the signal efficiency, also referred to as *signal-specific normalization*, caused by spectral differences between data and MC simulations.

The first two were evaluated in previous analyses [2], and are presented in Table I along with the other three, explained below. Table II shows the contribution of each constraint to the 90% CL limits (derived in Sec. V and shown in Fig. 2), evaluated by setting a negligible error to the constraint in the fit.

The uncertainty in SS fractions was evaluated using calibration data and was defined as the weighted average of the SS fractions residuals ((data-MC)/MC), with weights based on the signal spectrum and detector live-time. Since the SS fraction is observed to depend on energy, being $\gtrsim 90$% for energies below 700 keV for all components, this error was considered as the largest between those evaluated in energy and standoff-distance projections. The resulting SS-fraction constraint for each search is shown in Table I.

Imperfections in the MC model, common to all components, translate into an overall difference in number of events between data and MC prediction. This overall efficiency uncertainty is acccounted for by an additional degree of freedom added to the fitting PDF through a normalization parameter that scales all PDF coefficients equally. This normalization factor is constrained to unity within the estimated systematic error, whose largest contributions arise from the FV cut and the 3D clustering step of the reconstruction [5]. Using a similar approach as in previous analyses, these errors were found to be 5.8% (3.6%) and 2.3% (3.1%), respectively, for the $2\nu\beta\beta$ ($0\nu\beta\beta$) analysis. Other sources were found to contribute negligibly ($\lesssim 1$%) to the total normalization error, shown in Table I.

Discrepancies in the shape distributions between data and MC are propagated into the signal rate through a normalization parameter that only scales the coefficient of the signal PDFs. This signal-specific normalization parameter is constrained to unity within the errors arising from spectral shape agreement and background model.

To estimate the effect of shape errors, the ratio between data and MC of the projections onto energy, shown in Fig. 1, and standoff-distance were used to weight all PDF components (also referred to as *un-skewing*). The standoff-distance ratios, as well as those for energies above 850 keV, were found to be negligible contributors. ^{60}Co and ^{238}U-related PDFs were weighted by ratios using data from the calibration sources ^{60}Co and ^{226}Ra, respectively, while the other γ-like PDFs were weighted by ratios obtained with a ^{228}Th source. β-like PDFs were weighted using ratios from the background subtracted ^{136}Xe-$2\nu\beta\beta$ spectrum (Fig. 1), since these are also uniformly distributed in LXe. Approximately 10,000 toy datasets were drawn from these un-skewed PDFs, which were scaled by values arising from a data fit by the background-only model (without a signal PDF), while the number of signal counts included in the toy fits was manually set. These toy data sets were then fit using the normal PDFs and the average difference (bias) between the manually set and best-fit number of signal counts determined. This bias was found to be roughly constant at 2250 cts (240 cts) for the $2\nu\beta\beta$ ($0\nu\beta\beta$) analysis. The difference between these factors demonstrates the impact of the spectral discrepancy at low energies.

The dependence of the signal rate on the completeness of the fit model was studied by individually including possible background contributors in different locations and/or from other decays. The relative change of the estimated rate was then determined. This change was found to be negligible for ^{39}Ar and ^{42}Ar dissolved in the LXe, and for ^{60}Co and ^{238}U in components farther than the TPC vessel. The dominant contribution to this term in the $2\nu\beta\beta$ search arose from ^{210}Bi (10%), while in the $0\nu\beta\beta$ search ^{85}Kr in the LXe (12%) dominated. The impact of the ^{85}Kr on the $2\nu\beta\beta$ search is discussed in Sec. V.

The total deviations arising from background model uncertainties are shown in Table I (a), along with the estimated errors from the spectral agreement (b). The signal-specific normalization error is the largest systematic contribution in both searches, as presented in Table II, contributing to 34.6% (30.4%) increase of the 90% CL limit derived for ^{134}Xe $2\nu\beta\beta$ ($0\nu\beta\beta$).

Table I. Summary of the constraints added to the searches of $\beta\beta$ decays in ^{134}Xe. The signal-specific normalization error is calculated by $\sigma = \sqrt{(a \cdot n)^2 + b^2}$, where n is the number of signal counts.

Constraint	$2\nu\beta\beta$	$0\nu\beta\beta$
Radon in the LXe	10%	10%
Neutron-capture PDF fractions	20%	20%
SS fractions	5.7%	2.3%
Normalization	6.2%	4.9%
Signal-specific normalization	$a = 11.8\%$ $b = 2250$ cts	$a = 12.7\%$ $b = 240$ cts

Table II. Contribution of each systematic error to the 90% CL limits derived in the searches of ^{134}Xe $\beta\beta$-decays, presented in Sec. V.

Error Contribution	$2\nu\beta\beta$	$0\nu\beta\beta$
Radon in the LXe	$< 0.1\%$	$< 0.1\%$
Neutron-capture PDF fractions	$< 0.1\%$	$< 0.1\%$
SS fractions	16.6%	10.2%
Normalization	1.0%	0.2%
Signal-specific normalization	34.6%	30.4%

V. RESULTS AND DISCUSSION

Figure 2 shows the profile-likelihood scan performed for the ^{134}Xe $2\nu\beta\beta$ and $0\nu\beta\beta$ decays, where the lower limits of $T^{2\nu\beta\beta}_{1/2} > 8.7 \cdot 10^{20}$ yr and $T^{0\nu\beta\beta}_{1/2} > 1.1 \cdot 10^{23}$ yr at 90% CL are derived for their half-lives, respectively. The corresponding experimental sensitivities were evaluated at $1.2 \cdot 10^{21}$ yr and $1.9 \cdot 10^{23}$ yr, respectively. The results of the NLL fit from the ^{134}Xe $2\nu\beta\beta$ search are presented in Fig. 3, along with the fitted ^{134}Xe $0\nu\beta\beta$ from the other search. The limits presented in this paper increase the sensitivity relative to those available in the current literature by 5 orders of magnitude for the $2\nu\beta\beta$ search [10], while the limit set for $0\nu\beta\beta$ is nearly twice as stringent than the one in [12].

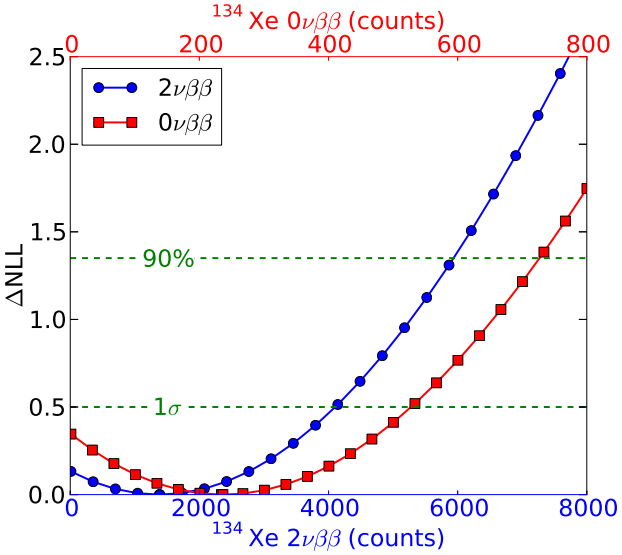

Figure 2. Profile-likelihood ratio, ΔNLL, for ^{134}Xe $2\nu\beta\beta$ and $0\nu\beta\beta$. The dashed lines represent the 1σ and 90% CLs, assuming the validity of Wilks's theorem [22, 23]. The latter intersects the profile curves at 5900 and 730 counts for $2\nu\beta\beta$ and $0\nu\beta\beta$, respectively.

The significance of the presence of a signal relative to the null hypothesis is calculated using fits of toy data sets and comparing the NLL between hypotheses. The p-values were found to be 0.24 and 0.19 for the $2\nu\beta\beta$ and $0\nu\beta\beta$ searches, respectively, showing that there is no statistically significant evidence for a non-zero signal.

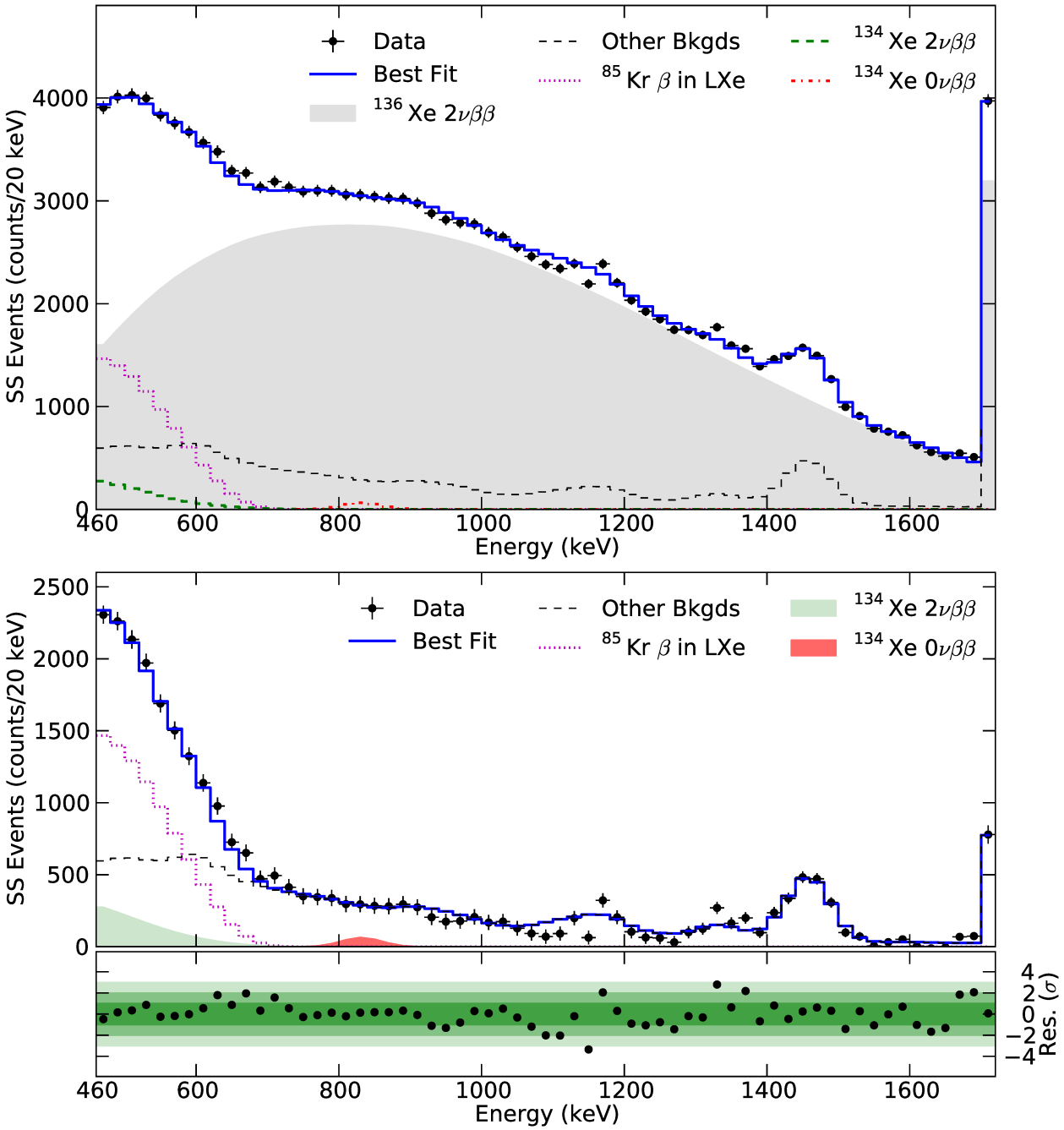

Figure 3. The top plot shows the SS energy projection for the results of the ^{134}Xe-2$\nu\beta\beta$ analysis, using the fitted central values. While the 0$\nu\beta\beta$ search is performed in a separate fit with higher energy threshold, it is overlaid here for comparison since the backgrounds at these energies are the same. The last bin is the summed contents of all bins between 1700 keV and 9800 keV. The middle plot shows the same results where the ^{136}Xe-2$\nu\beta\beta$ component is subtracted from data and best fit values. The bottom plot presents the residuals between data and best fit normalized to the Poisson error.

Both fitted β-scales are consistent with unity to the subpercent level. The fitted half-life of 2$\nu\beta\beta$ of ^{136}Xe agrees to better than 1% with its precise measurement in [2], which was obtained with a different analysis on a subset of the present data. The observed residuals from both analyses are comparable to those in [5], performed with a reduced data set.

Figure 4 shows the contour lines of the profile-likelihood ratio scanned for ^{85}Kr β and ^{134}Xe 2$\nu\beta\beta$. The solid lines were evaluated incorporating all the systematic errors in the NLL function, exactly as in the ^{134}Xe 2$\nu\beta\beta$ search, whereas the dashed lines were obtained without

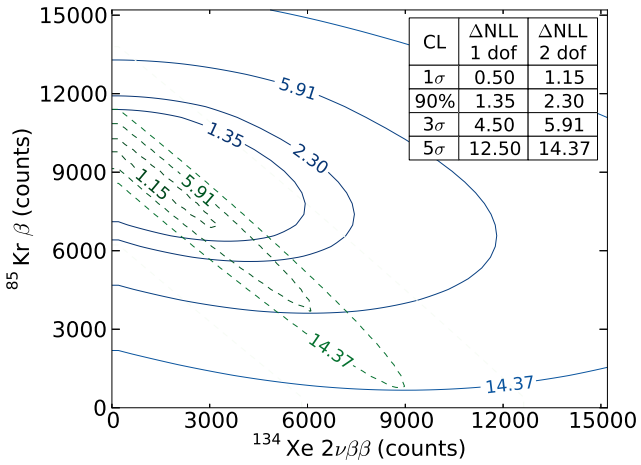

CL	ΔNLL 1 dof	ΔNLL 2 dof
1σ	0.50	1.15
90%	1.35	2.30
3σ	4.50	5.91
5σ	12.50	14.37

Figure 4. Contour lines of the profile-likelihood ratio, ΔNLL, scanned for the ^{85}Kr β and ^{134}Xe $2\nu\beta\beta$ components using two NLL functions. The blue solid lines were obtained using the same function as the ^{134}Xe $2\nu\beta\beta$ search, which accounts for all the systematic errors. The green dashed lines were evaluated without consideration of the normalization errors. The table shows ΔNLL values of various CL for 1 and 2 dof.

consideration of either the normalization error nor the signal-specific one. The latter better represents the large correlation between the two PDFs, $\rho = -0.97$, as expected from their shapes presented in Fig. 3, and shows the extent to which they are not fully degenerate. Contour lines for 2 degrees of freedom (dof) were evaluated, showing the regions where both variables are contained with corresponding CL. The data prefer non-zero ^{85}Kr β counts, which was checked to be driven by SS shape differences. As a result, the upper limit set on ^{134}Xe $2\nu\beta\beta$, 5900 cts, is improved by a factor of nearly two, if compared to the limit that would be set by the sum of components, estimated by the intersection of the solid ΔNLL = 2.30 line and the y-axis, 12000 cts.

A contamination of 25.5 ± 3 ppt natural krypton in the enriched LXe was measured before filling the TPC [25]. Combined with the current work, which does not perform a complete measurement of the ^{85}Kr contamination, these results suggest an isotopic abundance in the enriched LXe consistent with those at atmospheric levels, $\sim 10^{-11}$ g ^{85}Kr/g $^{\text{nat.}}$Kr [26]. Since the right edge of the solid lines can be identified with the profile depicted in Fig. 2, contour lines for 1 dof were also evaluated in this case. Thus, the impact of ^{85}Kr β in the ^{134}Xe-$2\nu\beta\beta$ limit can be estimated by its difference to the limit that would be set for a fixed amount of ^{85}Kr β. Considering this value to be that near the NLL minimum, 9000 cts, the solid ΔNLL = 1.35 line in Fig. 4 indicates a contribution of about 15% increase in the ^{134}Xe-$2\nu\beta\beta$ 90% CL upper limit. Further, as might be expected given the very different energy response, the impact of this uncertainty on the $0\nu\beta\beta$ search limit is significantly smaller.

EXO-200 has begun Phase-II data taking, after a two-year hiatus, with upgraded electronics that may result in better detection efficiency at low energies as well as improved spectral agreement between data and MC simulation. These improvements can positively impact future EXO-200 searches for $\beta\beta$-decay of ^{134}Xe. In the long term, the proposed nEXO detector is projected to increase the EXO-200 sensitivity to $0\nu\beta\beta$ in ^{136}Xe by nearly 3 orders of magnitude [27]. While the sensitivity for $\beta\beta$-decay in ^{134}Xe has not been directly studied yet, a similar increase in performance for ^{134}Xe would allow this next generation experiment to probe the $2\nu\beta\beta$ decay of this isotope to half-lives within the theoretical expectations.

ACKNOWLEDGMENTS

The EXO-200 collaboration acknowledges the KARMEN collaboration for supplying the cosmic-ray veto detectors, and the WIPP for their hospitality. EXO-200 is supported by DOE and NSF in the United States, NSERC in Canada, SNF in Switzerland, IBS in Korea, RFBR in Russia, DFG Cluster of Excellence "Universe" in Germany, and CAS and ISTCP in China. EXO-200 data analysis and simulation uses resources of the National Energy Research Scientific Computing Center (NERSC).

[1] C. Patrignani *et al.*, Chin. Phys. C, **40**, 100001 (2016).
[2] J. B. Albert *et al.* (EXO-200 Collaboration), Phys. Rev. C, **89**, 015502 (2014).
[3] J. Schechter and J. W. F. Valle, Phys. Rev. D, **25**, 2951 (1982).
[4] A. Gando *et al.* (KamLAND-Zen Collaboration), Phys. Rev. Lett, **117**, 082503 (2016).
[5] J. B. Albert *et al.* (EXO-200 Collaboration), Nature, **510**, 229 (2014).
[6] M. Wang *et al.*, Chin. Phys. C, **36**, 1603 (2012).
[7] B. Pontecorvo, Phys. Lett. B, **16**, 630 (1968).
[8] M. Duerr *et al.*, Phys. Rev. D, **84**, 093004 (2011).
[9] M. Redshaw *et al.*, Phys. Rev. Lett., **98**, 053003 (2007).
[10] A. Barabash *et al.*, Phys. Lett. B, **223**, 273 (1989).
[11] N. Barros *et al.*, J. Phys. G, **41** (2014).
[12] R. Bernabei *et al.*, Phys. Lett. B, **527**, 182 (2002).
[13] J. B. Albert *et al.* (EXO-200 Collaboration), Phys. Rev. D, **90**, 092004 (2014).
[14] J. B. Albert *et al.* (EXO-200 Collaboration), Phys. Rev. D, **93**, 072001 (2016).
[15] J. Severinghaus, Private Communication.
[16] J. B. Albert *et al.* (EXO-200 Collaboration), JCAP, **04**, 029 (2016).
[17] M. Auger *et al.* (EXO-200 Collaboration), JINST, **7**,

P05010 (2012).
[18] E. Conti *et al.*, Phys. Rev. B, **68**, 054201 (2003).
[19] J. Allison *et al.*, IEEE Trans. Nucl. Sci., **53**, 270 (2006).
[20] J. B. Albert *et al.* (EXO-200 Collaboration), Phys. Rev. C, **95**, 025502 (2017).
[21] C. G. Davis *et al.* (EXO-200 Collaboration), JINST, **11**, P07015 (2016).
[22] S. S. Wilks, Ann. Math. Statist., **9**, 60 (1938).
[23] G. Cown, *Statistical Data Analysis*, Oxford science publications (Clarendon Press, 1998).
[24] E. J. Konopinski, *The Theory of Beta Radioactivity* (Oxford University Press, New York, 1966).
[25] A. Dobi *et al.*, Nucl. Inst. & Meth. A, **675**, 40 (2012).
[26] P. Collon *et al.*, Ann. Rev. Nucl. Part. Sci., **54**, 39 (2004).
[27] C. Licciardi, *The Sensitivity of the nEXO Experiment to Majorana Neutrinos*, in proceedings of XXVII International Conference on Neutrino Physics and Astrophysics.